



A numerical analysis of developing flow and heat transfer in a curved annular pipe

M.R.H. Nobari*, B.R. Ahrabi¹, G. Akbari¹

Department of Mechanical Engineering, Amirkabir University of Technology, 424 Hafez Ave., P.O. Box 15875-4413, Tehran, Iran

ARTICLE INFO

Article history:

Received 12 April 2008

Received in revised form 9 December 2008

Accepted 10 December 2008

Available online 31 December 2008

Keywords:

Annular curved pipe

Incompressible flow

Finite difference

Projection method

ABSTRACT

Developing incompressible viscous fluid flow and heat transfer in a curved annular pipe is studied numerically. The governing equations consisting of continuity, full Navier–Stokes, and energy equations are solved using a projection method based on the second order central difference discretization. Considering the outer wall to be adiabatic, two different thermal boundary conditions involving constant temperature and constant heat flux are applied at the inner wall to analyze the heat transfer rate in the two different cases. The effects of governing non-dimensional parameters involving the aspect ratio, the curvature, Reynolds number, Dean number, and Prandtl number on the flow and temperature field both in developing and fully developed regions of the curved annular pipe are studied in detail. Two major different developing patterns of the flow are determined based on the location of maximum axial velocity either in the semi-inner or in the semi-outer region of the curved annular pipe. Also the numerical results obtained indicate that the friction factor and the Nusselt number in a curved annular pipe are both proportional to the square root of Dean number ($\kappa^{1/2}$). At $\kappa^{1/2} \leq 8$ the friction factor for both curved and straight annular pipes are the same, beyond that it increases in the circular curved pipe by increasing Dean number and decreasing aspect ratio.

© 2008 Elsevier Masson SAS. All rights reserved.

1. Introduction

Flow and heat transfer in curved pipes are used in a very large number of cases such as piping systems, bio-fluid mechanics especially blood flow in catheterized artery, engineering devices such as heat exchangers, cooling systems of rotating electrical machinery, chemical mixing or drying machinery, chemical reactors, chromatography columns, and other processing equipment. Because of the wide range of applications, flow and heat transfer in this configurations are studied extensively during the last decades.

Physical aspects of the fluid flow inside the curved pipes are very much complicated due to the presence of curvature generating centrifugal and pressure forces in the curvature direction. In contrast to the centrifugal forces, the pressure forces decrease in the curvature direction as the fluid particles approach centre of curvature. Mutual effects of centrifugal, pressure, inertia and viscous forces provide a very complex flow pattern which has not physically fully understood. A relatively detailed qualitative physical description of the flow in a plain curved pipe has been carried out by Yao and Berger [1]. However, shifting from a plain curved pipe flow to the annular one makes the flow pattern more com-

plex owing to the presence of an additional internal curved pipe. In this case the secondary boundary layers start developing on the walls of both curved pipes from their outermost point of curvatures, where the pressure forces are more than the centrifugal forces. On the other hand, in the core region off the two pipe walls, the reverse fluid motion, i.e. from the inner to the outer radii of curvature, occurs resulting from the larger centrifugal and smaller pressure forces. This secondary core flow which starts from the symmetrical plane at the inner radii of the curvature ($\phi = \pi$) develops similar to a jet flow and interacts with opposite flowing secondary boundary layers forming two pairs of vortices, a weak pair close to the inner pipe and a strong one close to the outer pipe. This phenomenon implies a physical point that in the secondary flows the diffusion of viscous forces occurs more rapidly than the main axial flow owing to the presence of small inertia forces (order of magnitude of secondary inertia forces is about 10^{-1} of the axial one). Within the entrance length up to the fully developed region, the centre location of vortices displace under the effect of the main axial flow development. At low Dean numbers (or low Reynolds numbers) and curvatures this displacement is small and the centre of large vortices along with the maximum axial velocity stay in the inner half curved pipe region (region 1 in Fig. 1), but the centre of small ones appear in the very beginning of the outer half curved region (region 2 in Fig. 1). Otherwise, as the larger the dean number and the curvature, this displacement becomes larger with the chance of breaking vortices into small ones. In these cases max-

* Corresponding author.

E-mail address: mnrnobi@aut.ac.ir (M.R.H. Nobari).

¹ Graduate student.

Nomenclature

c_p	specific heat at constant pressure
D_i	inner diameter of annular pipe
D_o	outer diameter of annular pipe
D_h	hydraulic diameter, $D_h = D_o - D_i$
f	frictional resistance
FR	friction factor, f_c/f_s
k	thermal conductivity
\mathbf{N}	outward normal unit vector to the boundary
\bar{Nu}	average Nusselt number
Nu	local Nusselt number
p	dimensionless pressure
Pr	Prandtl number, $Pr = \nu/\alpha$
q_w	heat flux at the inner wall of annular pipe
r	dimensionless radial coordinate
r_i	inner radius of annular pipe
r_o	outer radius of annular pipe
R_c	curvature radius
Re	Reynolds number, $Re = w_m D_h/\nu$
t	dimensionless time
T	dimensionless temperature
T_m	bulk fluid temperature
u, v, w	dimensionless velocity components in r, ϕ and θ direction, respectively
\mathbf{V}	velocity vector
w_m	mean axial velocity

Greek symbols

α	thermal diffusivity
δ_c	curvature ratio, $\delta_c = r_o/R_c$
δ_r	aspect ratio, $\delta_r = r_i/r_o$
θ	curvature coordinate
κ	Dean number, $\kappa = 2\delta_c^{1/2}(w_m D_h/\nu)$
μ	viscosity of fluid
ν	kinematic viscosity
ρ	density of fluid
τ	stress
ϕ	angular coordinate
Γ	boundary

Subscripts

c	curved annular pipe
fd	fully developed
i	inner wall
in	inlet of pipe
o	outer wall
s	straight annular pipe

Superscript

'	dimensional parameters
---	------------------------

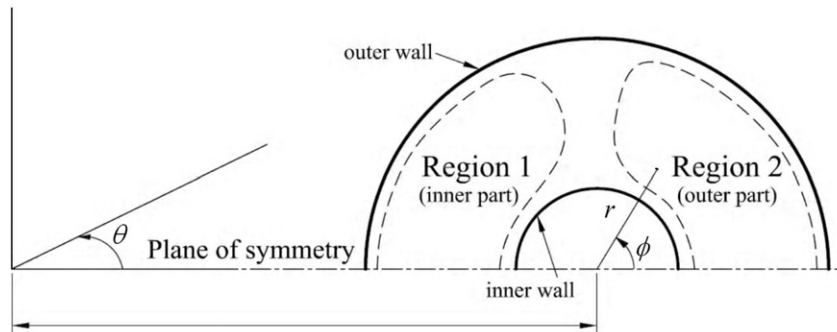


Fig. 1. Toroidal coordinates and geometry of the curved annular pipe.

imum axial flow velocity stays in region 2. Considering the main flow in the entrance region, at low Reynolds numbers (low Dean numbers) the growth rate of the main boundary layers ($\sim 1/\sqrt{Re}$) are larger resulting in the faster full diffusion of viscosity effects in the main flow and shorter entrance length. However, this is reverse in the higher Reynolds numbers at which the maximum axial velocity appears in the outer half curvature region (region 2). As the main flow starts developing from the entrance of the curved annular pipes toward the fully developed region, due to shifting the peaks of the main flow from the inner curved region toward the outer, the boundary layer thicknesses become thicker on the walls with the lower radii of the curvature and thinner on the walls with the higher radii of curvature. Based on the physical descriptions outlined above, the presence of the secondary flows in the curved pipes delays the development of the main flow by deforming the evolution of the axial velocity profile and increases the resistant of the fluid flow. Consequently, comparing to the similar straight pipes the reduction of flow rate and the increase of both friction rate and entrance length can be easily expected.

Many analytical, numerical and experimental works about the fluid flow and heat transfer in curved pipes are developed. The first

major study on the flow in the curved pipe was made by Dean [2,3] who considered a loosely curved pipe where the flow depends on a single non-dimensional parameter, i.e. the Dean number, $K = 2a/R(w_{\max}a/\nu)^2$, where a is the radius of pipe, R is the radius of curvature, w_{\max} is the maximum axial velocity in the corresponding straight pipe, and ν is the kinematic viscosity. Dean's work is valid for $K \leq 576$. In later works on curved pipes, a variety of Dean numbers have been used by different researchers. For example, McConalogue and Srivastava [4] proposed the parameter $D = (Ga^2/\mu)(2a^3/\nu^2R)^{1/2}$, where G is the constant pressure gradient along the pipe. This parameter relates to K as $D = 4K^{1/2}$. By this definition of Dean number, the upper limit of Dean's work becomes 96. They considered intermediate range of Dean numbers ($96 \leq D \leq 600$) using Fourier series method to formulate the problem and solve the resulting equations numerically. Collins and Dennis [5], and Dennis [6] used finite difference method to solve the flow equations in the range of $96 \leq D \leq 5000$. An investigation on developing laminar flow in a curved pipe was made by Soh and Berger [7] using artificial compressibility technique. They reported their results for $108.2 \leq \kappa \leq 680.3$, where $\kappa = 2\delta^{1/2}(W_m a/\nu)$ is another definition of Dean number. They found that curvature ratio

has great effect on the intensity of secondary flow and the separation which occurs near the inner wall of curved pipe. Among other similar works on flow in a stationary curved pipe, the works of Pedley [8], Dennis and Ng [9], Ito [10] and Kao [11] can be mentioned.

Nobari and Gharali [12] have investigated the effect of internal fins on the fluid flow and heat transfer through a rotating straight pipe and a stationary curved pipe. Ishigaki [13–15] examined flow and heat transfer in a rotating curved pipe and investigated the effect of Coriolis force in complicating the flow structure. Heat transfer and fluid flow in a curved annular pipe has been studied in the fully developed region by Karahalios [16], Petrakis and Karahalios [17]. Also, the effect of catheterization on the flow characteristics in a curved artery was studied by Karahalios [18], Ebadian [19], Jayaraman and Tiwari [20] and Dash et al. [21].

In the present work, direct numerical simulation of developing incompressible viscous flow and heat transfer in a curved annular pipe is studied using a projection algorithm based on the second order finite difference discretization. For doing so, a three-dimensional staggered grid in a toroidal coordinate system is used to discretize the governing equations including continuity, full Navier–Stokes and energy equations. To study heat transfer, two different thermal boundary conditions consisting of constant temperature and constant heat flux at the inner wall are applied. At both of these conditions, the outer wall of annular pipe is assumed to be adiabatic. The effects of governing non-dimensional parameters, such as Dean number, κ , Reynolds number, Re , curvature ratio, δ_c , and aspect ratio, δ_r , on the flow characteristics involving axial flow, secondary flow pattern, friction factor, temperature profiles and Nusselt number are investigated in details. It should be mentioned that developing flow in a curved annular pipe with a detailed physical analysis of the fully developed region is carried out for the first time in this study to the best of our knowledge.

2. Governing equations

Here, developing incompressible viscous fluid flow and heat transfer in a stationary curved annular pipe with circular cross section are studied. The best coordinate system compatible with the geometry of the physical domain is the toroidal coordinates system as shown in Fig. 1. Consequently, the governing equations describing the flow and heat transfer consisting of continuity, Navier–Stokes and energy equations are written in the toroidal coordinates system as non-dimensional form using the following non-dimensional parameters

$$\begin{aligned} r &= \frac{r'}{D_h}, & u &= \frac{u'}{w_m}, & v &= \frac{v'}{w_m} \\ w &= \frac{w'}{w_m}, & p &= \frac{p'}{\rho w_m^2}, & t &= \frac{t'}{D_h/w_m} \\ Re &= \frac{w_m D_h}{\nu}, & Pr &= \frac{\nu}{\alpha}, & \kappa &= 2\delta_c^{1/2} (W_m D_h/\nu) \\ T &= \frac{T' - T'_{in}}{T'_{in} - T'_{w}} \text{ for Case A,} & T &= \frac{T' - T'_{in}}{q_w D_h/k} \text{ for Case B} \end{aligned} \quad (1)$$

where, r is the dimensionless radial coordinate, D_h the hydraulic diameter of annular pipe ($D_o - D_i$), u the dimensionless velocity in the radial coordinate (r), w_m the mean axial velocity, v the dimensionless velocity in the angular coordinate (θ), w the dimensionless velocity in the curvature coordinate (ϕ), p the dimensionless pressure, ρ the density, t the dimensionless time, Re the Reynolds number, ν the kinematic viscosity, Pr the Prandtl number, α the thermal diffusivity, κ the Dean number, δ_c the curvature ratio ($\delta_c = r_o/R_c$), T the temperature, T'_{in} the inlet temperature,

T'_w the wall temperature of the inner pipe, k the thermal conductivity of the fluid, and q_w the constant heat flux at the inner pipe wall.

Therefore, the corresponding non-dimensional governing equations in the toroidal coordinate system can be expressed as

continuity

$$\frac{\partial}{\partial r}(r\xi u) + \frac{\partial}{\partial \theta}(\xi v) + \frac{\partial}{\partial \phi}(\delta r w) = 0 \quad (2)$$

r momentum

$$\begin{aligned} \frac{\partial u}{\partial t} + \frac{1}{r\xi} \left[\frac{\partial}{\partial r}(r\xi u^2) + \frac{\partial}{\partial \phi}(\xi uv) + \frac{\partial}{\partial \theta}(\delta ruw) - \xi v^2 - \delta r \cos \phi w^2 \right] \\ = -\frac{\partial p}{\partial r} + \frac{1}{Re} \left\{ \frac{1}{r\xi} \left[\frac{\partial}{\partial r} \left(r\xi \frac{\partial u}{\partial r} \right) + \frac{\partial}{\partial \phi} \left(\xi \frac{\partial u}{\partial \phi} \right) + \frac{\partial}{\partial \theta} \left(\frac{\delta^2 r}{\xi} \frac{\partial u}{\partial \theta} \right) \right] \right. \\ \left. - \frac{1}{r^2} \left(2 \frac{\partial v}{\partial \phi} + u \right) + \frac{\delta \sin \phi v}{r\xi} \right. \\ \left. + \frac{\delta^2 \cos \phi}{\xi^2} \left(v \sin \phi - u \cos \phi - 2 \frac{\partial w}{\partial \theta} \right) \right\} \end{aligned} \quad (3)$$

ϕ momentum

$$\begin{aligned} \frac{\partial v}{\partial t} + \frac{1}{r\xi} \left[\frac{\partial}{\partial r}(r\xi uv) + \frac{\partial}{\partial \phi}(\xi v^2) + \frac{\partial}{\partial \theta}(\delta rvw) - \xi uv + \delta r \sin \phi w^2 \right] \\ = -\frac{1}{r} \frac{\partial p}{\partial \phi} + \frac{1}{Re} \left\{ \frac{1}{r\xi} \left[\frac{\partial}{\partial r} \left(r\xi \frac{\partial v}{\partial r} \right) + \frac{\partial}{\partial \phi} \left(\xi \frac{\partial v}{\partial \phi} \right) + \frac{\partial}{\partial \theta} \left(\frac{\delta^2 r}{\xi} \frac{\partial v}{\partial \theta} \right) \right] \right. \\ \left. + \frac{1}{r^2} \left(2 \frac{\partial u}{\partial \phi} - u \right) - \frac{\delta \sin \phi u}{r\xi} \right. \\ \left. - \frac{\delta^2 \sin \phi}{\xi^2} \left(v \sin \phi - u \cos \phi - 2 \frac{\partial w}{\partial \theta} \right) \right\} \end{aligned} \quad (4)$$

θ momentum

$$\begin{aligned} \frac{\partial w}{\partial t} + \frac{1}{r\xi} \left[\frac{\partial}{\partial r}(r\xi uw) + \frac{\partial}{\partial \phi}(\xi vw) + \frac{\partial}{\partial \theta}(\delta_c r w^2) \right. \\ \left. - \delta r w(u \cos \phi - v \sin \phi) \right] \\ = -\frac{\delta}{\xi} \frac{\partial p}{\partial \theta} + \frac{1}{Re} \left\{ \frac{1}{r\xi} \left[\frac{\partial}{\partial r} \left(r\xi \frac{\partial w}{\partial r} \right) + \frac{\partial}{\partial \phi} \left(\xi \frac{\partial w}{\partial \phi} \right) \right. \right. \\ \left. \left. + \frac{\partial}{\partial \theta} \left(\frac{\delta^2 r}{\xi} \frac{\partial w}{\partial \theta} \right) \right] + \frac{2\delta^2}{\xi^2} \left(\frac{\partial u}{\partial \theta} \cos \phi - \frac{\partial v}{\partial \theta} \sin \phi - \frac{w}{2} \right) \right\} \end{aligned} \quad (5)$$

energy

$$\begin{aligned} \frac{\partial T}{\partial t} + u \frac{\partial T}{\partial r} + \frac{v}{r} \frac{\partial T}{\partial \phi} + \frac{\delta}{\xi} w \frac{\partial T}{\partial \theta} \\ = \frac{1}{Pr \cdot Re} \frac{1}{r\xi} \left[\frac{\partial}{\partial r} \left(r\xi \frac{\partial T}{\partial r} \right) + \frac{\partial}{\partial \phi} \left(\xi \frac{\partial T}{\partial \phi} \right) + \delta^2 \frac{\partial}{\partial \theta} \left(\frac{r}{\xi} \frac{\partial T}{\partial \theta} \right) \right] \end{aligned} \quad (6)$$

where, $\xi = 1 + \delta r \cos \phi$ and $\delta = D_h/R_c$.

As it is clear from Eqs. (3) to (6), here, the transient equations are used to reach the steady state solution because of the simplicity of the parabolic equations comparing with the elliptic ones. Furthermore, the flow field is symmetric relative to the horizontal mid plane, and it is enough to take into account either upper or lower semicircle region of the curved annular pipe in the numerical simulation. Therefore, the following four boundary conditions can be applied.

At the inlet:

uniform axial flow

$$w(r, \phi, 0) = 1, \quad u(r, \phi, 0) = 0, \quad v(r, \phi, 0) = 0 \quad (7)$$

and uniform temperature

$$T(r, \phi, 0) = 1 \quad \text{for Case A}$$

$$T(r, \phi, 0) = 0 \quad \text{for Case B}$$

At the outlet:

hydrodynamically fully developed

$$\frac{\partial u}{\partial \theta} = \frac{\partial v}{\partial \theta} = \frac{\partial w}{\partial \theta} = 0 \quad \text{at } \theta = \theta_{fd} \quad (9)$$

and thermally fully developed

$$\begin{aligned} \frac{\partial T}{\partial \theta} &= \frac{T}{T_m} \frac{\partial T_m}{\partial \theta} && \text{for Case A} \\ \frac{\partial T}{\partial \theta} &= \frac{dT_w}{d\theta} = \frac{4\delta_r}{Re Pr \delta_c (1 - \delta_r^2)} && \text{for Case B at } \theta = \theta_{fd} \end{aligned} \quad (10)$$

where, θ_{fd} is sufficient enough to consider the flow fully developed both hydrodynamically and thermally. Depending on the amount of Reynolds and Dean numbers, the values of π and $3\pi/2$ for θ_{fd} are used in the fully developed region.

At the walls:

no slip conditions for velocity

$$\begin{aligned} \text{inner wall: } u(r_i, \phi, \theta) &= v(r_i, \phi, \theta) = w(r_i, \phi, \theta) = 0 \\ \text{outer wall: } u(r_o, \phi, \theta) &= v(r_o, \phi, \theta) = w(r_o, \phi, \theta) = 0 \end{aligned} \quad (11)$$

where,

$$r_i = \frac{r'_i}{D_h} = \frac{\delta_r}{2(1 - \delta_r)}, \quad r_o = \frac{r'_o}{D_h} = \frac{1}{2(1 - \delta_r)} \quad (12)$$

constant temperature at the inner wall and adiabatic outer wall (Case A)

$$\begin{aligned} T &= 0 \quad \text{at } r = r_i \\ \frac{\partial T}{\partial r} &= 0 \quad \text{at } r = r_o \end{aligned} \quad (13)$$

or constant heat flux at the inner wall and adiabatic outer wall (Case B)

$$\begin{aligned} \frac{\partial T}{\partial r} &= -1 \quad \text{at } r = r_i \\ \frac{\partial T}{\partial r} &= 0 \quad \text{at } r = r_o \end{aligned} \quad (14)$$

Plane of symmetry:

$$\begin{aligned} \frac{\partial u}{\partial \phi} &= \frac{\partial w}{\partial \phi} = \frac{\partial T}{\partial \phi} = 0 \quad \text{and} \\ v &= 0 \quad \text{at } \phi = 0, \pi \end{aligned} \quad (15)$$

3. Numerical method




In this study the projection method which is introduced by Chorin [22] for the first time is employed to solve the transient Navier–Stokes equations using forward in time and central in space finite difference discretization. Although the unsteady solutions are physically accurate here, the concentration is focused on the steady state solutions where the transient terms vanish. In the projection algorithm, the Navier–Stokes and continuity equations are written as:

$$\frac{\mathbf{V}^{n+1} - \mathbf{V}^n}{\Delta t} + \mathbf{A}(\mathbf{V}^n) + \nabla p^{n+1} = \frac{1}{Re} \nabla^2 \mathbf{V}^n \quad (16)$$

$$\nabla \cdot \mathbf{V}^{n+1} = 0 \quad (17)$$

Table 1

Grid independence test for three different grid sizes ($\delta_r = 0.2$, $\delta_c = 1/7$, $Re = 200$ and $Pr = 5$) at Case A.

Grid size	FR	w_{max}	Nu_c/Nu_s	Axial velocity contours
30 × 20 × 30	1.0517	1.6889	1.3066	
50 × 30 × 40	1.0672	1.6961	1.3245	
80 × 40 × 80	1.0685	1.6968	1.3261	

Then, defining the temporary velocity, \mathbf{V}^* , Eq. (20) can be split into Eqs. (22) and (23)

$$\frac{\mathbf{V}^* - \mathbf{V}^n}{\Delta t} + \mathbf{A}(\mathbf{V}^n) - \frac{1}{Re} \nabla^2 \mathbf{V}^n = 0 \quad (18)$$

$$\frac{\mathbf{V}^{n+1} - \mathbf{V}^*}{\Delta t} + \nabla p^{n+1} = 0 \quad (19)$$

Taking the divergence of Eq. (19) and using Eq. (17) leads to the Poisson equation for the pressure:

$$\nabla^2 p^{n+1} = \frac{1}{\Delta t} \nabla \cdot \mathbf{V}^* \quad (20)$$

The Neumann condition for the pressure at the boundary is obtained by projecting Eq. (19) normal to the boundaries

$$\left(\frac{\partial p}{\partial n} \right)_\Gamma^{n+1} = -\frac{1}{\Delta t} (\mathbf{V}_\Gamma^{n+1} - \mathbf{V}_\Gamma^*) \cdot \mathbf{n} \quad (21)$$

where, the subscript Γ indicates the boundary. It can be shown that the pressure field is independent of \mathbf{V}_Γ^* , therefore, by choosing $\mathbf{V}_\Gamma^* = \mathbf{V}_\Gamma^{n+1}$, zero pressure gradient is obtained on the boundaries. Due to explicit discretization, the following stability conditions must be satisfied

$$\begin{aligned} \frac{\Delta t}{Re \min\{(R d\theta)^2, (r d\phi)^2, (dr)^2\}} &\leq 1/6 \\ \max(u^2 + v^2 + w^2) Re \Delta t &\leq 2 \end{aligned} \quad (22)$$

To obtain a physical pressure field, a staggered uniform grid in which no pressure nodes exist on the boundaries is used.

For the grid independence test of the numerical code implemented, three different grid sizes shown in Table 1 are considered to compare the numerical results obtained in fully developed region in the case of constant heat flux at the inner wall (Case A). The comparison of the friction factors, Nusselt numbers, mean temperatures and the axial velocity contours clearly indicates the conservative property of the developed numerical code and its grid independent results, where the maximum error is about 1.5%. Finally, it should be declared that the maximum error of the residuals to reach to the steady state solution is assumed to be of the order of 1×10^{-6} .

4. Results and discussion

To verify the accuracy of the code implemented here, a high curvature case ($\delta_c = 1/100$) which is too close to the straight concentric pipe is simulated, and the results obtained are compared with the analytical solution in the fully developed region in Fig. 2

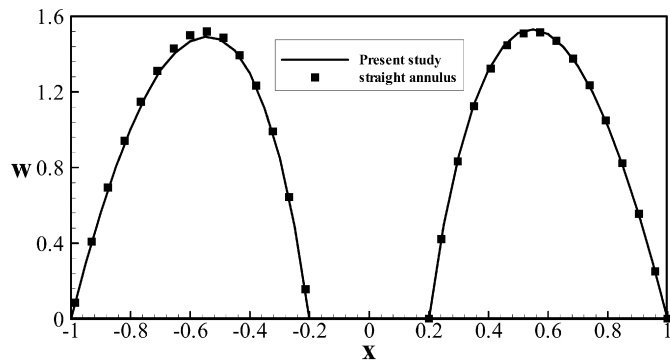


Fig. 2. Comparison between axial velocity in the plane of symmetry of a curved annular pipe with $\delta_c = 100$ and analytical solution of similar straight one.

indicating a very good agreement. Now, the numerical results obtained for the flow and heat transfer in the curved annular pipe at different curvatures and aspect ratios are described in detail at the following. First the flow field is analyzed and then the corresponding results obtained for heat transfer will be taken into account.

4.1. Axial flow development

Fig. 3 shows the axial flow development on the symmetry plane for a curved annular pipe with $\delta_r = 0.2$ and $\delta_c = 1/7$ at different Reynolds numbers. Due to curvature and no slip conditions at the inner and outer walls, the development of the axial velocity is affected by the interaction of the main and secondary flow boundary layers. The numerical results obtained here indicate that the axial flow pattern is different for low Reynolds numbers from high

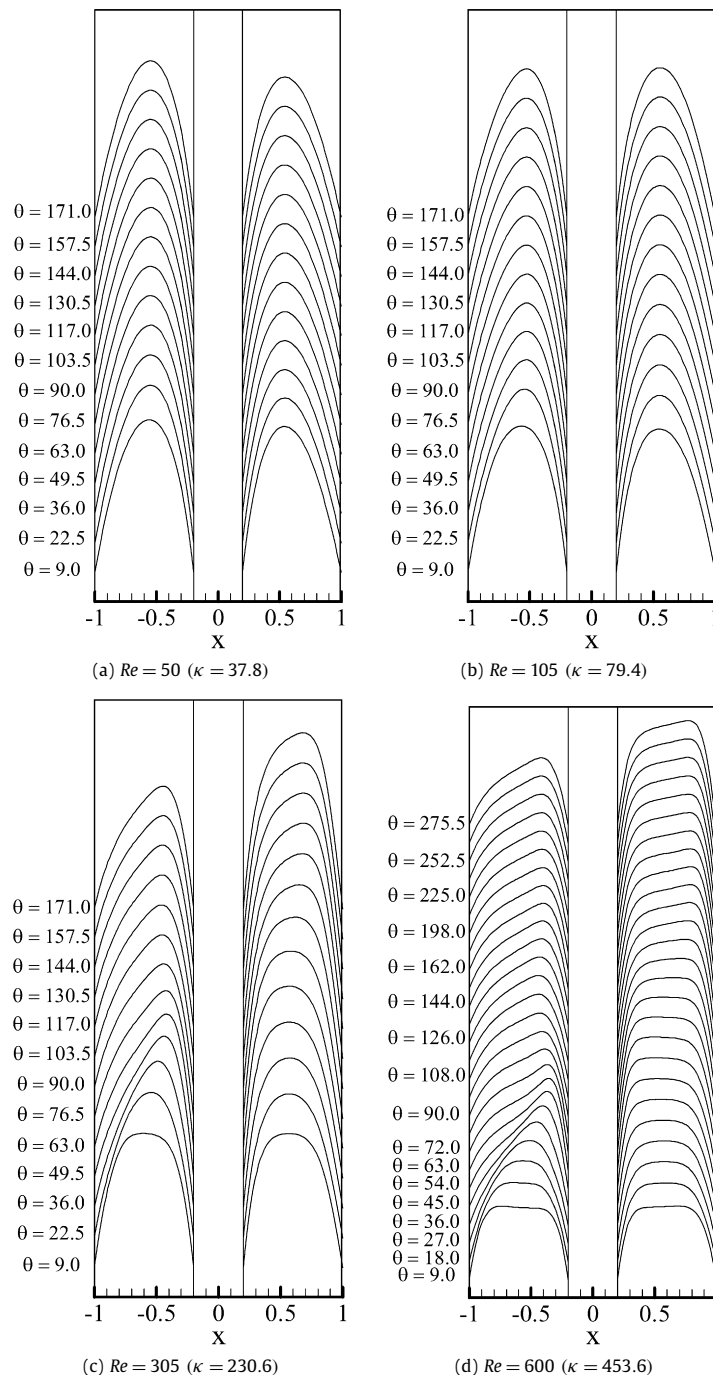
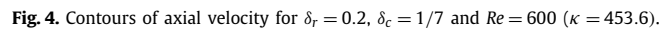


Fig. 3. Development history of axial velocity on the plane of symmetry for $\delta_r = 0.2$, $\delta_c = 1/7$.



Because of presence of the inner pipe in annular curved pipes, the development of the fluid flow follows different pattern of evolution from the one in a single curved pipe, and the maximum axial velocity and its location in the fully developed region is a function of Re , δ_c and δ_r . In Fig. 5 the variation of w_{\max} versus Re at different aspect ratios is shown for an annular pipe with $\delta_c = 1/7$. The physics of this phenomenon can be explained considering the role of viscous, inertia, and centrifugal forces in developing fluid flow in region 1, the half pipe towards inner, and region 2, the half pipe towards outer. At low Reynolds numbers, due to large viscous forces centrifugal forces become dominant in region 1 causing the fluid accumulates in that region where the maximum axial velocity appears (Fig. 3a). As Reynolds number increases, the amount of dominant centrifugal forces in region 1 decreases while the centrifugal forces in region 2 increases. This physical trend reduces the amount of fluid accumulation in region 1 causing the reduction of maximum velocity located in that region. At a specified Reynolds number depending on the δ_c and δ_r ($Re = 135$ at $\delta_r = 0.4$ and $Re = 70$ at $\delta_r = 0.2$ in Fig. 5) the centrifugal forces in the two regions balance each other providing uniform distribution of fluid in the annular curved pipe where the maximum axial velocity becomes minimum and appears in the both regions at the whole annular pipe. In this case the axial velocity profile in the curved annular pipe is similar to the one in the straight annular pipe but with the peak close to the inner pipe wall not at midsection of the annular pipe. Beyond this Reynolds number,

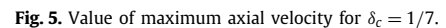


Fig. 6 shows the secondary flow streamlines in different cross sections of the curved annular pipe. The centrifugal forces generated due to the curvature of the annular curved pipe results in developing secondary flows and deflecting the axial velocity profile comparing with the straight pipes. As it is clear from Fig. 6, at the near entrance of the annular curved pipe first the two pairs of Dean vortices are created, one large pair around the outer pipe and one small pair around the inner pipe, then downstream towards fully developed region depending on the Reynolds number different evolution of vortices occurs. At low Reynolds numbers (Fig. 6a), downstream towards the fully developed region, the core of large pair of vortices moves to region 1 where the maximum

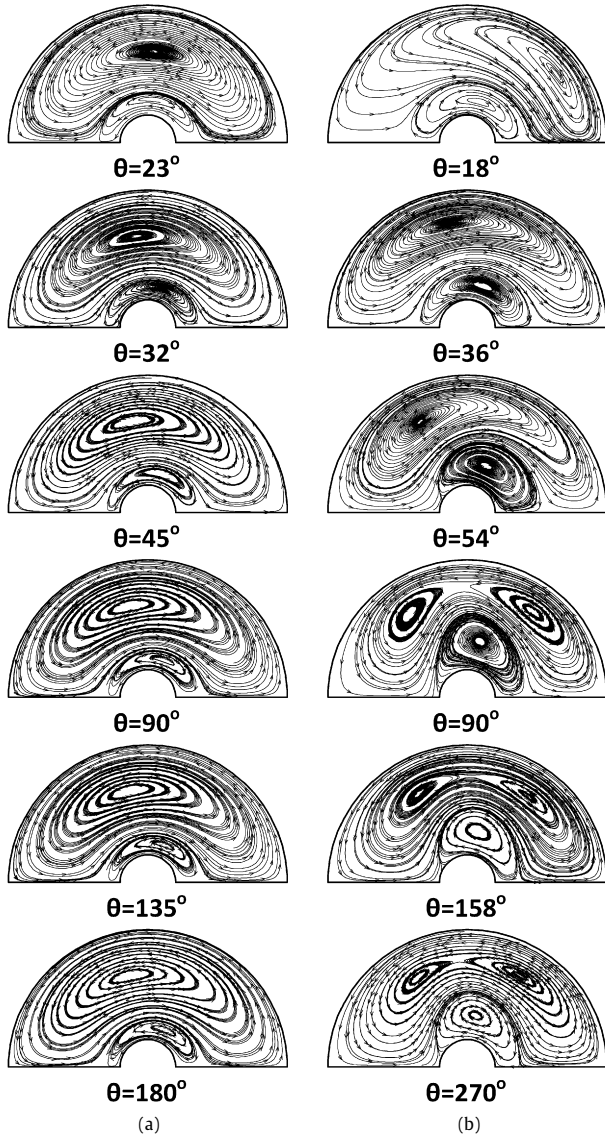


Fig. 6. Secondary flow streamlines for $\delta_r = 0.2$, $\delta_c = 1/7$, (a) $Re = 50$ and $\kappa = 37.8$ (left column), (b) $Re = 600$ and $\kappa = 453.6$ (right column).

axial velocity is located, but the core of small pair of vortices stays in region 2. However, at high Reynolds numbers, the two stronger pairs of vortices generated break into two or more small pairs of vortices depending on the Reynolds number. As an example, in Fig. 6b for the case of $\delta_r = 0.2$, $\delta_c = 1/7$ and $Re = 600$, the large pair of vortices are split into two pairs of vortices, one pair greater in region 2 and the other pair smaller in region 1. But small pair of vortices stays unsplit with their cores in region 2.

4.2. Shear stresses and friction factor

Due to the secondary flows generated by centrifugal forces in the curved pipes, circumferential boundary layers in addition to axial boundary layers develop. The two shear stresses governing the flow in a curved pipe can be expressed as

$$\tau_{r\phi} = \frac{\partial v}{\partial r}, \quad \tau_{r\theta} = \frac{\partial w}{\partial r} \quad (23)$$

In Fig. 7 the variation of circumferential shear stress on the walls of the inner and outer curved pipes are shown in fully developed region for a curved annular pipe with $\delta_r = 0.2$, $\delta_c = 1/7$, and $\kappa = 453.6$ at $Re = 600$ (solid lines). As the figure indicates,

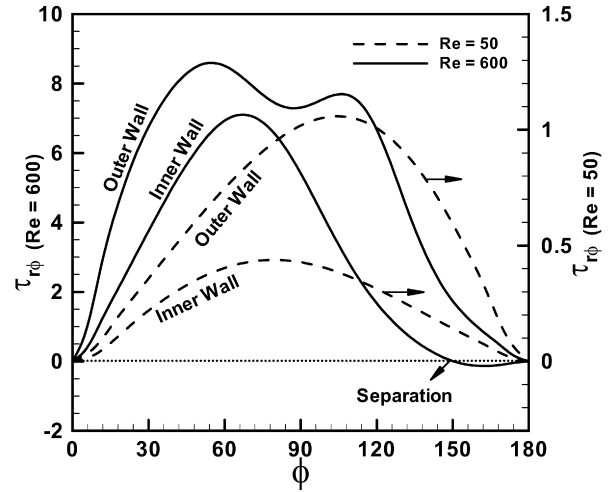


Fig. 7. Circumferential shear stress in fully developed region for $\delta_r = 0.2$, $\delta_c = 1/7$, solid lines (left vertical axis) indicate the case of $Re = 600$ ($\kappa = 453.6$), and dash lines (right vertical axis) indicate the case of $Re = 50$ ($\kappa = 37.8$).

there are two peaks for the shear stress on the outer pipe wall corresponding to the ϕ angles where the cores of the two vortices around the outer pipe wall are located (Fig. 6b). But at the inner pipe wall due to a single small vortex, there is only one peak for the shear stress which is located at the ϕ angle related to the small vortex core as shown in Fig. 6b. Also a separation point where the shear stress vanishes is traced on the inner pipe wall. At these peak points, the circumferential boundary layer thickness becomes thinner than others due to the local higher inertia forces. Furthermore, because of larger centrifugal forces around the outer pipe, the values of shear stress on the outer pipe wall are higher than the ones on the inner pipe wall. At low Reynolds and Dean number, the circumferential stresses are also shown in Fig. 7 (dash lines) where only one peak appears on the outer pipe wall due to a single vortex formation on it (Fig. 6a).

The friction factor in the flow inside pipes is one the most important physical parameters which must be taken into account. Here the ratio of the friction factor for curved annular pipe to the one for the straight annular pipe is taken into account as

$$FR = \frac{f_c}{f_s} = \frac{\int_0^{2\pi} (\tau_{r\theta}(r_o, \phi, \theta_{fd}) \cdot r_o + \tau_{r\theta}(r_i, \phi, \theta_{fd}) \cdot r_i) d\phi}{\int_0^{2\pi} (\tau_{r\theta}(r_o, \phi, \theta_{fd}) \cdot r_o + \tau_{r\theta}(r_i, \phi, \theta_{fd}) \cdot r_i) d\phi} \quad (24)$$

or

$$FR = \frac{f_c}{f_s} = \frac{\frac{\partial p}{\partial \theta}|_{fd,c}/R_c}{\frac{\partial p}{\partial z}|_{fd,s}} \quad (25)$$

where f_c and f_s are the friction factors for the curved and straight pipes respectively.

Following the above mentioned formulas, the numerical results for the friction factor ratio versus square root of Dean number are shown in Fig. 8 for six different cases including three different aspect ratios of 0.2, 0.4, and 0.6 at two different curvatures of 1/7 and 1/15. As the figure indicates, by variation of curvature the friction factor remains constant, exploring that the friction factor in the curved pipes can only be expressed as a function of the square root of the Dean number. However, as δ_r increases the friction factor decreases resulting from the reduction of centrifugal effects and the dominant effect of viscous forces. Another important point can be found from Fig. 8 is that for $\kappa^{1/2} \leq 8$, the friction factor in the curved annular pipe approaches to the one in the similar straight pipe and becomes independent of the curvature.

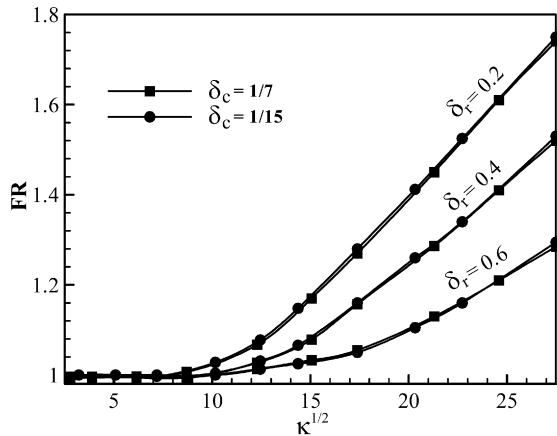


Fig. 8. Friction factor versus square root of Dean number.

4.3. Temperature field and heat transfer rate

In addition to the non-dimensional parameters considered in the fluid flow of the curved annular pipe, Prandtl number has to be taken into account in heat transfer analysis. Two different thermal boundary conditions depending on whether the inner pipe wall to be at constant temperature (Case A) or constant heat flux (Case B) are considered while the outer pipe wall is kept adiabatic in both cases. The temperature field pattern depends on the behavior of centrifugal forces resulting from the curvature of the pipe.

To investigate heat transfer in the developing region, a circumferentially averaged Nusselt number at each cross-section of the pipe is defined as

$$\overline{Nu}_{(\theta)} = \frac{1}{\pi d_1} \int_0^{2\pi} Nu_{(\phi, \theta)} r_i d\phi = \frac{1}{2\pi} \int_0^{2\pi} Nu_{(\phi, \theta)} d\phi \quad (26)$$

Since the outer wall is kept adiabatic, its Nusselt number is zero. Therefore, the Nusselt number is computed on the inner curved pipe wall for the two thermal boundary conditions mentioned above. In Fig. 9 circumferentially averaged Nusselt number variation along the axis of the curved pipe is shown for two different thermal boundary conditions at three Reynolds numbers of 100, 400 and 800. At low Reynolds numbers due to dominant viscous forces no fluctuations is observed for the peripherally averaged Nusselt number, but at large Reynolds numbers centrifugal forces are strong enough to fluctuate the averaged Nusselt number in the entrance region. As it is clear from the figure, in the fully developed region, the averaged Nusselt number becomes uniform and its value is always greater for the constant heat flux case than the constant temperature one. To investigate the effect of the aspect ratio and the curvature on the heat transfer rate, the circumferentially averaged Nusselt number is shown versus curved pipe axial direction in Fig. 10 where three different aspect ratios of 0.2, 0.4, and 0.6 including two different curvatures of 1/15 and 1/7 are taken into account. The numerical results indicate that as the aspect ratio increases the heat transfer rate decreases due to reduction of centrifugal forces, and as the curvature increases the heat transfer rate increases because of enhancement of centrifugal forces. To clarify the history of circumferentially local Nusselt number development in the entrance region, its variations at different axial positions are shown in Fig. 11 at two different Reynolds numbers of 400 and 800 with $\delta_r = 0.4$, $\delta_c = 1/7$ and $Pr = 5$. The minimum points in the figure are related to the separation points which occur on the inner pipe wall. It can be realized that as the Reynolds number increases this separation point moves towards downstream.

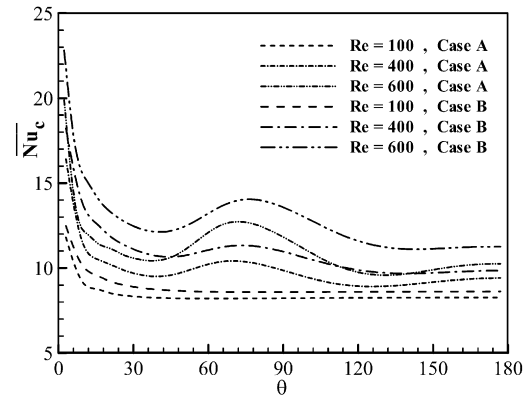


Fig. 9. Variation of average Nusselt number along the pipe axis at different Reynolds numbers for Cases A and B ($\delta_r = 0.2$, $\delta_c = 1/7$ and $Pr = 0.7$).

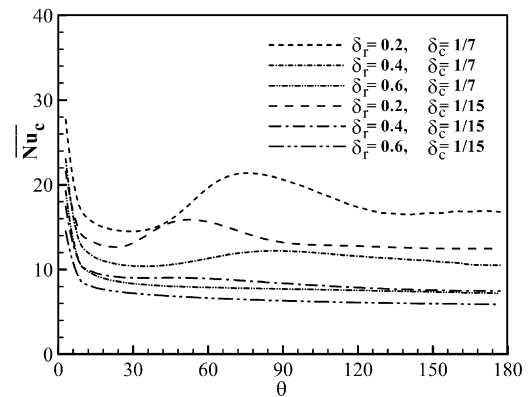


Fig. 10. Variation of average Nusselt number along the pipe axis at different aspect ratios and curvatures.

The fully developed results are commonly used in designing engineering systems; therefore, it must be paid close attention to the physical aspects of heat transfer occurring in the fully developed region. Fig. 12 illustrates the effects of the Reynolds and Prandtl variations on the circumferentially local Nusselt number in the fully developed region for the inner curved pipe. As it was shown earlier in the hydrodynamic results, at low Reynolds numbers the centrifugal forces are dominant in region 1 ($90^\circ \leq \phi \leq 180^\circ$) where the large vortex core and the maximum velocity occur. For this reason at $Re = 100$, the local Nusselt number monotonically increases at both Prandtl numbers of 0.7 and 5. But at higher Reynolds numbers the centrifugal forces are dominant in region 2 ($0^\circ \leq \phi \leq 90^\circ$) where the local Nusselt number becomes larger than region 1 where a minimum point due to separation occurs. To study the effects of the aspect ratio and curvature variations on the heat transfer, the circumferentially local Nusselt number on the inner curved pipe is shown at the three different aspect ratios and two different curvatures in Fig. 13 for the $Re = 400$ and $Pr = 5$. By increasing the curvature of the curved pipe the centrifugal forces become stronger, resulting in the increase of local Nusselt number. This phenomenon can be easily discovered in Fig. 13. The ratio of averaged circumferential Nusselt number in fully developed region of the curved annular pipe to that of similar straight annular pipe versus the Reynolds number is shown in Fig. 14 where both thermal boundary conditions are taken into account at the three different Prandtl numbers of 0.7, 5 and 30. As seen from the figure, the Nusselt number for the constant heat flux case is always greater than that for the constant temperature one, and for the higher Reynolds numbers depending on the Prandtl number the rate of heat transfer increases sharply because of stronger centrifugal effects. Also as the Prandtl number increases, the heat

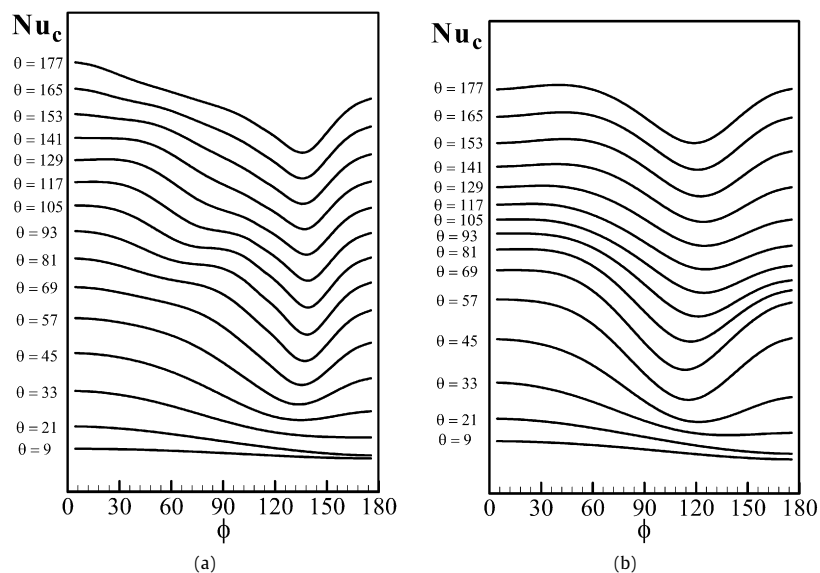


Fig. 11. Variation of local Nusselt number along the pipe axis for $Re = 400$ (a) and $Re = 800$ (b) at Case A ($\delta_r = 0.4$, $\delta_c = 1/7$ and $Pr = 5$).

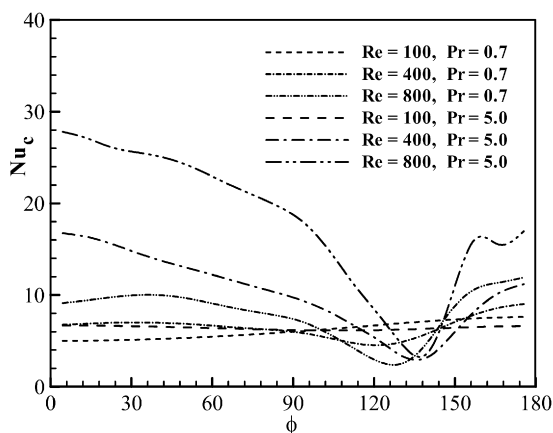


Fig. 12. Variation of local Nusselt number along the inner wall at different Reynolds and Prandtl numbers in fully developed region for Case A ($\delta_r = 0.4$ and $\delta_c = 1/7$).

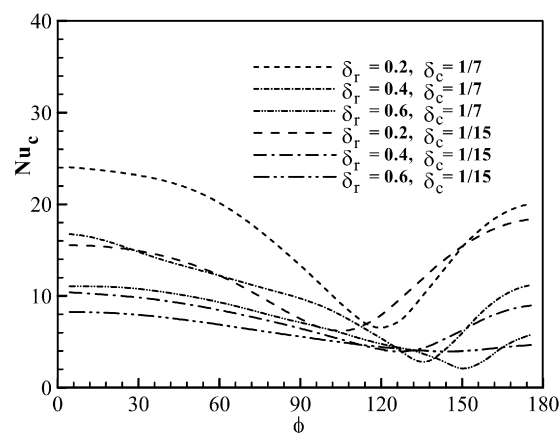


Fig. 13. Variation of local Nusselt number along the inner wall at different aspect ratios and curvatures in fully developed region for Case A ($Re = 400$ and $Pr = 5$).

transfer rate increases due to thin thermal boundary layer at the wall. At low Reynolds number depending on the Prandtl number, the heat transfer rate stays constant resulting from the large viscous forces and the small centrifugal forces effects. The variation of the averaged circumferential Nusselt number ratio versus the square root of Dean number is shown in Fig. 15 for case A at the Prandtl number of 5 with two different curvatures and three different aspect ratios. The numerical results obtained indicate that the Nusselt number in the fully developed can be expressed in terms of Dean number which takes into account both the curvature and the Reynolds number effects. As the aspect ratio increases, the simultaneous decreasing of the centrifugal effects and increasing of the viscous forces causes reduction in the heat transfer rate. For the case shown in Fig. 15, at $\kappa^{1/2} \leq 5$, the heat transfer rate of the curved annular pipe becomes equal to the similar straight pipe due to strong viscous forces.

The typical hydrodynamic and thermal entrance angles in degree are reported in Table 2 where the five different Reynolds numbers, two different curvatures, two different aspect ratios, and two different thermal boundaries are taken into account. The numerical values obtained indicate that the entrance length increases as the curvature, the Reynolds number (or Dean number), and the aspect ratio increase, but the increase rate due to curvature is more

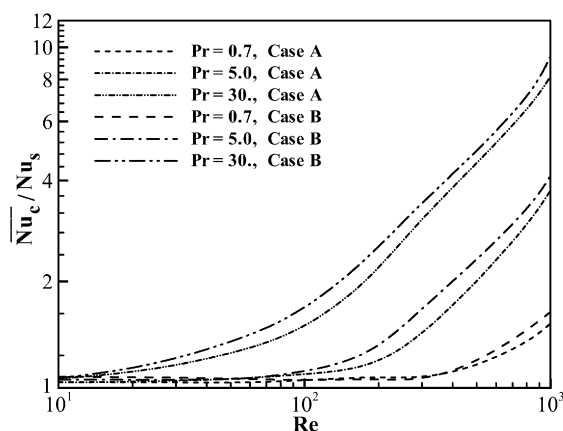
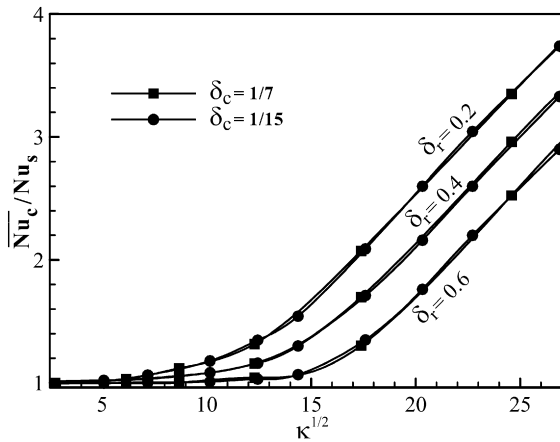


Fig. 14. Variation of \bar{Nu}_c/Nu_s versus Reynolds number in fully developed region at different Prandtl numbers for Cases A and B.

stronger than the other parameters. The typical values shown here provide significantly large entrance lengths comparing with the similar straight pipes requiring special attention when designing engineering equipment or studying the deposition of cholesterol in blood vessels.

Table 2Hydrodynamic (θ_{H-fd}) and thermal (θ_{T-fd}) entrance angles in annular curved pipes.

Re	θ_{H-fd}				θ_{T-fd} at constant temperature								θ_{T-fd} at constant heat flux							
	$\delta_c = 1/15$		$\delta_c = 1/7$		$\delta_c = 1/15$				$\delta_c = 1/7$				$\delta_c = 1/15$				$\delta_c = 1/7$			
	$\delta_r = 0.2$		$\delta_r = 0.4$		$\delta_r = 0.2$		$\delta_r = 0.4$		$\delta_r = 0.2$		$\delta_r = 0.4$		$\delta_r = 0.2$		$\delta_r = 0.4$		$\delta_r = 0.2$		$\delta_r = 0.4$	
	$Pr = 0.7$		$Pr = 5$		$Pr = 0.7$		$Pr = 5$		$Pr = 0.7$		$Pr = 5$		$Pr = 0.7$		$Pr = 5$		$Pr = 0.7$		$Pr = 5$	
	$\delta_r = 0.2$	$\delta_r = 0.4$	$\delta_r = 0.2$	$\delta_r = 0.4$	$\delta_r = 0.2$	$\delta_r = 0.4$	$\delta_r = 0.2$	$\delta_r = 0.4$	$\delta_r = 0.2$	$\delta_r = 0.4$	$\delta_r = 0.2$	$\delta_r = 0.4$	$\delta_r = 0.2$	$\delta_r = 0.4$	$\delta_r = 0.2$	$\delta_r = 0.4$	$\delta_r = 0.2$	$\delta_r = 0.4$	$\delta_r = 0.2$	$\delta_r = 0.4$
50	30	34	66	70	26	71	29	78	57	121	58	125	25	79	29	92	60	127	65	132
100	50	55	90	100	41	89	44	101	81	129	84	136	43	97	47	106	82	140	89	152
200	80	90	130	150	69	162	80	169	119	175	128	185	76	173	88	191	124	192	133	207
400	102	127	160	181	93	202	114	219	138	218	157	248	97	221	121	245	146	243	171	261
600	130	150	204	232	112	231	127	259	185	256	206	321	119	261	136	276	192	291	225	312

**Fig. 15.** Variation of \bar{Nu}_c/Nu_s versus square root of Dean number in fully developed region at different aspect ratios and curvatures for Case A with $Pr = 5$.

5. Summary and conclusion

Developing fluid flow and heat transfer in an annular curved pipe is studied numerically using projection method based on the second order finite difference discretization to solve the governing equations including continuity, full Navier–Stokes, and energy equations. The effects of non-dimensional parameters consisting of aspect ratio, curvature, Reynolds number, Dean number, Prandtl number on the friction coefficient and the heat transfer rate both in entrance and fully developed regions are studied in detail.

Two major flow field patterns in an annular curved pipe fluid flow are determined based on the location of the maximum axial velocity either in the semi-inner or in the semi-outer region of the annular pipe. At the low Reynolds numbers depending on the curvature the maximum axial velocity stays on the semi-inner portion of the annular curved pipe which is referred to as region 1 where the viscous forces dominate to the centrifugal forces generated due to the curvature of the annular curved pipe. When the centrifugal forces dominate to viscous forces, typically at $Re > 100$, the maximum axial velocity shifts from region 1 to region 2 which covers the semi-outer portion of the curved annular pipe. As the Reynolds number increases, the Dean vortices generated due to centrifugal forces at the outer and inner curved walls of the annular pipe become stronger and depending on the Reynolds number they break into two or more small vortices.

Both the friction coefficient and the Nusselt number in the fully developed region of the curved annular pipes depend on the Dean number which includes both the Reynolds and the curvature effects. The numerical results obtained indicate that at $\kappa^{1/2} \leq 8$ the

friction factor in the curved annular pipe becomes equal to the one in the similar straight annular pipe, but at $\kappa^{1/2} > 8$ the friction factor increases by increasing the Dean number and decreasing the aspect ratio. On the other hand, the Nusselt number for the curved annular pipe at $\kappa^{1/2} \leq 6$ is the same as straight annular pipe for $Pr = 5$. Beyond that the Nusselt number in the curved annular pipe increases by increasing the Dean number and decreasing aspect ratio.

References

- [1] L.S. Yao, S.A. Berger, Entry flow in a curved pipe, *J. Fluid Mech.* 67 (1975) 177–196.
- [2] W.R. Dean, Note on the motion of fluid in a curved pipe, *Phil. Mag.* 4 (1927) 208–223.
- [3] W.R. Dean, The stream-line motion of fluid in a curved pipe, *Phil. Mag.* 5 (1928) 673–695.
- [4] D.J. McConalogue, R.S. Srivastava, Motion of fluid in a curved tube, *Proc. Roy. Soc. London A* 307 (1968) 37–53.
- [5] W.M. Collins, S.C.R. Dennis, The steady motion of a viscous fluid in a curved tube, *Q. J. Mech. Appl. Math.* 28 (2) (1975) 133–156.
- [6] S.C.R. Dennis, Calculation of the steady flow through a curved tube using a new finite-difference method, *J. Fluid Mech.* 99 (1980) 449–467.
- [7] W.Y. Soh, S.A. Berger, Laminar entrance flow in a curved pipe, *J. Fluid Mech.* 148 (1984) 109–135.
- [8] T.J. Pedley, *The Fluid Mechanics of Large Blood Vessels*, Cambridge University Press, 1980.
- [9] S.C.R. Dennis, M. Ng, Dual solutions for steady laminar flow through a curved tube, *Q. J. Mech. Appl. Math.* 35 (1982) 305–324.
- [10] H. Ito, Flow in curved pipes, *JSME Int. J.* 30 (1987) 543–552.
- [11] H.C. Kao, Some aspects of bifurcation structure of laminar flow in curved ducts, *J. Fluid Mech.* 243 (1992) 519–539.
- [12] M.R.H. Nobari, K. Gharali, A numerical study of flow and heat transfer in internally finned rotating straight pipes and stationary curved pipes, *Int. J. Heat Mass Transfer* 49 (2006) 1185–1194.
- [13] H. Ishigaki, Fundamental characteristics of laminar flows in a rotating curved pipe, *Trans. JSME B* 59 (1993) 1494–1501.
- [14] H. Ishigaki, Laminar flow in rotating curved pipes, *J. Fluid Mech.* 329 (1996) 373–388.
- [15] H. Ishigaki, Laminar convective heat transfer in rotating curved pipes, *JSME Int. J. Ser. B* 42 (1999) 489–497.
- [16] G.T. Karahalios, Mixed convection flow in a heated curved pipe with core, *Phys. Fluids A* 2 (12) (1990) 2164–2175.
- [17] M.A. Petrakis, G.T. Karahalios, Fluid flow behaviour in a curved annular conduit, *Int. J. Non-Linear Mech.* 34 (1999) 13–25.
- [18] G.T. Karahalios, Some possible effect of a catheter on the arterial wall, *Med. Phys.* 17 (1990) 922–928.
- [19] M.A. Ebadian, Rate of flow in a concentric pipe of circular cross-section, *J. Appl. Mech.*, *Trans. ASME* 57 (1990).
- [20] G. Jayaraman, K. Tiwari, Flow in a catheterised curved artery, *Med. Biol. Eng. Comput.* 33 (5) (1995) 1–6.
- [21] R.K. Dash, G. Jayaraman, K.N. Mehta, Flow in a catheterised curved artery with stenosis, *J. Biomech.* 32 (1999) 49–61.
- [22] J.A. Chorin, Numerical solution of the Navier–Stokes equations, *Math. Comput.* 22 (104) (1968) 745–762.